Photophysics of the fluorescent pH Indicator BCECF

ARTICLE *in* THE JOURNAL OF PHYSICAL CHEMISTRY A · SEPTEMBER 2006

Impact Factor: 2.69 · DOI: 10.1021/jp0615712 · Source: PubMed

6 AUTHORS, INCLUDING:

Wenwu Qin
Lanzhou University
67 PUBLICATIONS **2,087** CITATIONS
SEE PROFILE

Angel Orte
University of Granada
66 PUBLICATIONS **1,176** CITATIONS
SEE PROFILE

Jose M Alvarez-Pez
University of Granada
63 PUBLICATIONS **918** CITATIONS
SEE PROFILE

Photophysics of the Fluorescent pH Indicator BCECF

Noël Boens,* Wenwu Qin, and Nikola Basarić

Department of Chemistry, Katholieke Universiteit Leuven, Celestijnenlaan 200F, 3001 Heverlee, Belgium

Angel Orte, Eva M. Talavera, and Jose M. Alvarez-Pez*

Department of Physical Chemistry, University of Granada, Cartuja Campus, Granada 18071, Spain

Received: March 14, 2006; In Final Form: June 7, 2006

The photophysical behavior of BCECF [2′,7′-bis-(2-carboxyethyl)-5-(and-6)-carboxyfluorescein]—currently the most widely used fluorescent pH indicator for near-neutral intracellular pH measurements—has been explored by using absorption and steady-state and time-resolved fluorescence measurements. The influence of ionic strength as well as total buffer concentration on the absorbance and steady-state fluorescence has been investigated. The apparent acidity constant of the pH indicator determined by absorbance and fluorescence titration is dependent on the added buffer and salt concentrations. A semiempirical model is proposed to rationalize the variations in the apparent pK_a values. The excited-state proton exchange of BCECF at physiological pH becomes reversible upon addition of phosphate buffer, inducing a pH-dependent change of the fluorescence decay times. Fluorescence decay traces collected as a function of total buffer concentration and pH were analyzed by global compartmental analysis yielding the following values of the rate constants describing excited-state dynamics of BCECF: $k_{01} = 3.4 \times 10^8\ s^{-1}$, $k_{02} = 2.6 \times 10^8\ s^{-1}$, $k_{21} \approx 1 \times 10^6\ M^{-1}\ s^{-1}$, $k_{12}^B = 1.4 \times 10^8\ M^{-1}\ s^{-1}$, and $k_{21}^B = 4.3 \times 10^7\ M^{-1}\ s^{-1}$.

1. Introduction

Fluorescent pH indicators are indispensable tools for measuring changes of intracellular proton concentrations.[1] To quantitatively determine pH, it is imperative to match the pK_a of the indicator to the pH of the investigated system. Because the pH in the cytosol is close to neutral (generally between ~6.8 and 7.4), fluorescent indicators with a pK_a around 7 are required for cytosolic pH determinations. The most frequently used fluorescent indicators for near-neutral pH measurements in cells are fluorescein-derived molecules.[1] Fluorescein, in aqueous solution, can exist in one or more of four different prototropic forms (cation, neutral, monoanion, and dianion) depending on pH.[2,3] In near-neutral solution, only the dianion and monoanion forms, with fluorescence quantum yields of 0.93 and 0.37, respectively, are important. Fluorescein itself is not often used for measuring intracellular pH, because its high leakage rate from cells makes it very difficult to quantify intracellular pH. Other dyes such as BCECF[4,5] are now preferred for intracellular pH measurements because they are better retained in cells than fluorescein. Even though BCECF has three additional carboxylic acid functional groups compared to fluorescein (see Figure 1), at near-neutral pH all carboxylic acid groups are deprotonated. Therefore, at near-neutral pH, one can expect a similar behavior for the prototropic forms of BCECF derived from proton exchange at the phenol functional group as for the monoanion and dianion forms of fluorescein. As with fluorescein, the absorption spectrum of the phenolate anion (basic) form of BCECF is red-shifted and has increased molar absorption coefficients relative to the phenol (acidic) form. Conversely, there is no pH-dependent shift of the fluorescence emission spectra of BCECF upon excitation at $\lambda_{ex} = 505$ nm. The excitation spectra at 535 nm show a pseudoisoemissive point around 440 nm as a function of pH. Intracellular pH measurements with BCECF are typically done in the dual-excitation ratiometric mode with $\lambda_{ex}{}^1/\lambda_{ex}{}^2 = 490/440$ nm.

Fluorimetric titrations as a function of pH are a useful method for determining the K_a value of the indicator. However, the protonation reaction is possible also in the excited state,[6,7] and this may lead to an erroneous value of K_a derived from fluorimetric titrations. To fully understand the complex photophysics of BCECF, it is essential to elucidate the excited-state dynamics of the molecular forms present at near-neutral pH. Rate constants of all excited-state processes and spectral parameters associated with excitation and emission are the relevant parameters to be determined. Although there have been numerous reports on the use of BCECF for measuring intracellular pH, a detailed investigation of its photophysics has not been described (only values of the fluorescence lifetimes of BCECF have been reported[8]).

The single-photon timing (or time-correlated single-photon counting) technique[9,10] supplies time-resolved fluorescence data from which the relevant photophysical parameters can be obtained. To decide on the most suitable model to describe a specific photophysical system, a multidimensional fluorescence decay surface is measured under various experimental conditions. For the model of excited-state proton dissociation in the presence of added buffer—considered in this paper—the experimental variables are the excitation (λ_{ex}) and emission (λ_{em}) wavelengths, pH, and buffer concentration C^B. In many instances, the fluorescence response after a short excitation pulse can be analyzed in terms of a limited number of decay times τ_i and their associated amplitudes α_i. An accurate estimation of the τ_i and α_i values can be realized by the global analysis approach, in which the decay times τ_i can be linked (e.g., over

* To whom correspondence should be addressed. E-mail: Noel.Boens@chem.kuleuven.be (N.B.), jalvarez@ugr.es (J.M.A.-P.).

10.1021/jp0615712 CCC: $33.50
Published on Web 07/11/2006

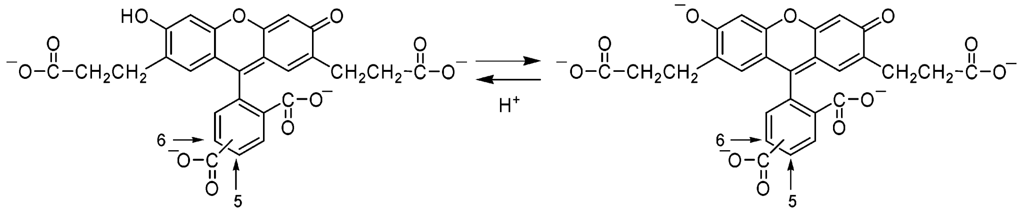

1 **2**

Figure 1. Chemical structures and ground-state proton exchange reaction of BCECF forms **1** (tetraanion) and **2** (pentaanion) at near-neutral pH.

decay traces collected at various emission wavelengths).[11−13] For decays collected at various pH, however, τ_i generally varies and hence cannot be linked. The empirical parameters $\{\tau_i, \alpha_i\}$ are not the primary parameters of interest. The more fundamental underlying parameters are kinetic (rate constants k_{ij}) and spectral parameters related to excitation ($\tilde{b}_1$) and emission ($\tilde{c}_1$). The power of global compartmental analysis derives specifically from the fact that one fits directly for these underlying parameters. Indeed, it allows the direct estimation of the parameters of interest from the complete fluorescence decay surface in a single step.[14−17]

Recently, we studied the fluorescence kinetics, the deterministic and the numerical identifiability of the model of intermolecular excited-state proton dissociation reaction in the absence and presence of added pH buffer.[18−20] A model is said to be uniquely (or globally) identifiable if the parameters of the assumed model can be uniquely determined from the idealized experiment. Without added buffer, the decay times τ_i ($i = 1, 2$) are independent of pH, and the model is not identifiable. An infinite number of model parameter estimates fitting the data makes the considered model unidentifiable. When a pH buffer is added to this photophysical system, the proton transfer becomes reversible and the model becomes uniquely identifiable under the following conditions. To have a uniquely identifiable model, at least three fluorescence decays should be collected, characterized by at least two different pH values and at least two different nonzero buffer concentrations. In addition to these three traces, minimally one biexponential fluorescence decay of the pH probe in the absence of buffer has to be recorded to determine all rate constants describing the excited-state events (k_{ij}). Furthermore, for the accurate estimation of k_{ij}, $\tilde{b}_1$, and $\tilde{c}_1$, at least two of these decay traces should be collected at the same pH and excitation and emission wavelengths. For the widely used fluorescent pH probes with p$K_a \approx 7$ that are responsive in the near-neutral pH range, it is advisable to use buffers with pK_a^B values comparable to or somewhat higher than the pK_a of the probe to have a maximal effect on $\{\tau_i, \alpha_i\}$.[20] For BCECF with a reported pK_a of 7.0,[4] we therefore chose phosphate buffer ($H_2PO_4^-/HPO_4^{2-}$) with p$K_a^B = 6.82$ at 20 °C, MOPS [3-(*N*-morpholino)propanesulfonic acid] with pK_a^B = 7.15 at 20 °C, and TRIS [tris(hydroxymethyl)aminomethane] with p$K_a^B = 8.08$ at 20 °C.

In this paper, we first explore the ground-state equilibrium between the tetraanionic (structure **1** in Figure 1) and pentaanionic (structure **2** in Figure 1) forms of BCECF through absorption measurements. Second, the influence of the addition of salt and buffer on the apparent acidity constant of BCECF measured via absorption and fluorescence titrations is investigated. Finally, the excited-state dynamics of the indicator in the presence of phosphate buffer is investigated in detail using global compartmental analysis of the fluorescence decay surface collected as a function of emission wavelength (λ_{em}), pH, and buffer concentration (C^B).

SCHEME 1: Representation of the Kinetic Model of Ground and Excited-state Proton- Exchange Reactions in the Presence of pH Buffer[a]

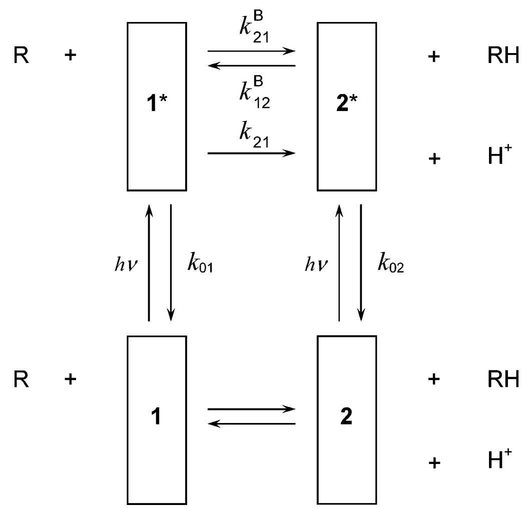

[a] **1** and **2** are, respectively, the ground-state acid (tetraanion) and conjugate base (pentaanion) forms of the fluorescent pH indicator BCECF, and **1*** and **2*** are the associated excited species. RH and R denote, respectively, the acid and conjugate base forms of the buffer. In the time-resolved experiments of BCECF, RH is $H_2PO_4^-$, and R is HPO_4^{2-}. The ground-state forms **1** and **2** of BCEF are shown in Figure 1.

2. Theory

2.1. Fluorescence Decay Kinetics. Consider a causal, linear, time-invariant, intermolecular system consisting of two distinct types of ground-state forms of a pH indicator and two corresponding excited-state species as shown in Scheme 1. Ground-state species **1** can deprotonate to form ground-state species **2** and H^+. For BCECF at near-neutral pH, species **1** and **2** are depicted in Figure 1. The proton-exchange reaction is described by the ground-state acidity constant $K_a = [\mathbf{2}][H^+]/[\mathbf{1}]$ of the pH indicator. Photoexcitation creates the excited-state species **1*** and **2***, which can decay by fluorescence (F) and nonradiative (NR) processes. The composite rate constants for these processes are denoted by k_{01} ($= k_{F1} + k_{NR1}$) and k_{02} ($= k_{F2} + k_{NR2}$). k_{21} stands for the rate constant for the dissociation of **1*** into **2*** and H^+. As only a pH probe useful at near-neutral pH will be considered in this paper, it will be assumed that $[H^+]$ is so small as to make the rate of association of $\mathbf{2}^* + H^+ \rightarrow \mathbf{1}^*$ negligible. The acidity of the buffer can be described by its ground-state acidity constant $K_a^B = [R][H^+]/[RH]$. In the ground state, the acidic form of the pH indicator (species **1**) can react with the basic form of the pH buffer (R) to give the basic form of the

pH probe (species **2**) and the acidic form of the buffer (RH). In the excited state, the reaction of **1*** with R to form **2*** and RH is characterized by rate constant k_{21}^{B}. The reverse reaction of **2*** and RH to give **1*** and R is described by rate constant k_{12}^{B}.

If the photophysical system shown in Scheme 1 is excited by an infinitely short light pulse that does not significantly alter the concentrations of the ground-state species (i.e., in the low excitation limit), then the fluorescence δ-response function, $f(\lambda_{em},\lambda_{ex},t)$, at emission wavelength λ_{em} due to excitation at λ_{ex} is given by[16]

$$f(\lambda_{em},\lambda_{ex},t) = \kappa\tilde{\mathbf{c}}(\lambda_{em})\mathbf{U}\exp(t\Gamma)\mathbf{U}^{-1}\tilde{\mathbf{b}}(\lambda_{ex},\mathrm{pH}) \quad t \geq 0 \qquad (1)$$

with κ a proportionality constant. $\mathbf{U} \equiv [\mathbf{U}_1, \mathbf{U}_2]$ is the matrix of the two eigenvectors of the compartmental matrix **A** (eq 2), and $\mathbf{U}^{-1}$ is the inverse of **U**, and $\exp(t\,\Gamma) \equiv \mathrm{diag}\,(\exp(\gamma_1 t), \exp(\gamma_2 t))$, with γ_1 and γ_2 being the eigenvalues of **A** corresponding to $\mathbf{U}_1$ and $\mathbf{U}_2$, respectively.

$$\mathbf{A} = \begin{bmatrix} -(k_{01} + k_{21} + k_{21}^{B}[\mathrm{R}]) & k_{12}^{B}[\mathrm{RH}] \\ k_{21} + k_{21}^{B}[\mathrm{R}] & -(k_{02} + k_{12}^{B}[\mathrm{RH}]) \end{bmatrix} \qquad (2)$$

$\tilde{\mathbf{b}}(\lambda_{ex},\mathrm{pH})$ is the 2×1 column vector with elements $\tilde{b}_i(\lambda_{ex},\mathrm{pH})$ defined by

$$\tilde{b}_i = b_i/(b_1 + b_2) \qquad (3)$$

where b_i denotes the concentration of i^* at time zero

$$b_i = [i^*]_{t=0} \qquad (4)$$

which in the low-excitation limit is proportional to the ground-state absorbance of i. Hence, $\tilde{b}_i$ represents the normalized absorbance of species i at λ_{ex}. The $\tilde{\mathbf{b}}(\lambda_{ex},\mathrm{pH})$ parameters can be expressed as a function of the ground-state acidity constant K_a of the pH indicator, the molar absorption coefficients $\epsilon_i(\lambda_{ex})$ of ground-state species i at λ_{ex}, and the pH of the sample solution. For $\tilde{b}_1(\lambda_{ex},\mathrm{pH})$ at $[H^+]$ and λ_{ex}, we have

$$\frac{1}{\tilde{b}_1(\lambda_{ex},\mathrm{pH})} = 1 + \frac{\epsilon_2(\lambda_{ex})K_a}{\epsilon_1(\lambda_{ex})[H^+]} \qquad (5)$$

$\tilde{\mathbf{c}}(\lambda_{em})$ is the 1×2 row vector of the normalized emission weighting factors $\tilde{c}_i(\lambda_{em})$ of species i^* at λ_{em}:[16]

$$\tilde{c}_i = c_i/(c_1 + c_2) \qquad (6)$$

The emission weighting factors $c_i(\lambda_{em})$ are given by[16]

$$c_i(\lambda_{em}) = k_{Fi}\int_{\Delta\lambda_{em}} \rho_i(\lambda_{em})\mathrm{d}\lambda_{em} \qquad (7)$$

k_{Fi} stands for the fluorescence rate constant of species i^*; $\rho_i(\lambda_{em})$ is the emission density of species i^* at emission wavelength λ_{em}, normalized to the complete steady-state fluorescence spectrum F_i of species i^*; $\Delta\lambda_{em}$ is the emission wavelength interval around λ_{em} where the fluorescence signal is monitored. $\rho_i(\lambda_{em})$ is defined by[16]

$$\rho_i(\lambda_{em}) = F_i(\lambda_{em})/\int_{\mathrm{fullband}} F_i\mathrm{d}\lambda_{em} \qquad (8)$$

Use of $\tilde{\mathbf{b}}$ and $\tilde{\mathbf{c}}$ in global compartmental analysis[14-17] allows one to link $\tilde{b}_1$ (i.e., $\tilde{b}_1$ is considered as a single estimable parameter in the curve-fitting) at the same pH and λ_{ex}, whereas $\tilde{c}_1$ can be linked at the same λ_{em}.

Equation 1 can be written in the common biexponential format:

$$f(\lambda_{em}, \lambda_{ex}, t) = \alpha_1 \exp(\gamma_1 t) + \alpha_2 \exp(\gamma_2 t) \quad t \geq 0 \qquad (9)$$

The eigenvalues $\gamma_{1,2}$ are given by[18,20]

$$\gamma_{1,2} = -\frac{1}{2}[(S_1 + S_2) \pm \sqrt{(S_1 - S_2)^2 + 4k_{12}^{B}[\mathrm{RH}](k_{21} + k_{21}^{B}[\mathrm{R}])}] \qquad (10)$$

with

$$S_1 = k_{01} + k_{21} + k_{21}^{B}[\mathrm{R}] \qquad (11a)$$

$$S_2 = k_{02} + k_{12}^{B}[\mathrm{RH}] \qquad (11b)$$

and are related to the decay times $\tau_{1,2}$ according to

$$\gamma_{1,2} = -1/\tau_{1,2} \qquad (12)$$

The exponential factors $\gamma_{1,2}$ (and hence also $\tau_{1,2}$) depend on pH, because [R] and [RH] are generally pH-dependent. Indeed, [R] and [RH] can be expressed as a function of $[H^+]$, K_a^B of the buffer, and the analytical buffer concentration C^B (= [R] +[RH]).[18,20]

$$[\mathrm{R}] = \frac{K_a^B C^B}{K_a^B + [H^+]} \qquad (13a)$$

$$[\mathrm{RH}] = \frac{[H^+]C^B}{K_a^B + [H^+]} \qquad (13b)$$

The preexponential factors $\alpha_{1,2}$ are dependent on the rate constants k_{ij}, pH, λ_{ex}, λ_{em}, and the total buffer concentration C^B.

When the pH is much higher than pK_a and pK_a^B, only species **2** and **2*** are present, and [RH] $\approx$ 0 (i.e., $C^B \approx$ [R]). In that case, the value of the amplitude α_1 associated with the limiting value of $\tau_1 = (k_{01} + k_{21} + k_{21}^B C^B)^{-1} = S_1^{-1}$ vanishes. Hence, the fluorescence δ-response function is given by eq 14

$$f(\lambda_{em}, \lambda_{ex}, t) = b_2\, c_2 \exp(-k_{02}t) \quad t \geq 0 \qquad (14)$$

and this assigns a unique value to k_{02}.

2.2. Determination of K_a and Molar Absorption Coefficients from Absorciometric Titration. The absorbance A of BCECF aqueous solutions depends on pH according to Beer's law and the simple acid−base equilibrium theory. To analyze the experimental absorbance vs pH, we implemented a global nonlinear least-squares curve fitting method. Assuming that the photophysical system follows Beer's law, at any wavelength λ_{abs} and pH, the absorbance A is given by the expression:

$$A(\mathrm{pH},\lambda_{abs}) = C^{\mathrm{BCECF}}(\sum_i \alpha_i(\mathrm{pH},pK_a^{app})\epsilon_i(\lambda_{abs}))d \qquad (15)$$

where C^{BCECF} is the total concentration of BCECF, d is the optical path length, $\epsilon_i(\lambda_{abs})$ is the molar absorption coefficient of the ith prototropic form of BCECF depending on wavelength, and $\alpha_i(\mathrm{pH}, pK_a^{app})$ is the fraction of BCECF in the ith prototropic form. The values of α_i depend on both pH and the apparent ground-state acidity constant (pK_a^{app} value) according to the simple acid−base equilibrium equations.

The nonlinear global fitting of the entire A vs pH vs λ_{abs} surface to eq 15 and the corresponding acid−base equilibrium equations allows the determination of the molar absorption coefficients $\epsilon_i(\lambda_{abs})$ and pK_a^{app}. In this global fitting, the apparent pK_a^{app} was a linked parameter over the whole surface, whereas $\epsilon_i(\lambda_{abs})$ were locally adjustable parameters at each wavelength for each species.

2.3. Determination of K_a from Direct Fluorimetric Titration. If the photophysical system depicted in Scheme 1 is excited with light of constant intensity, and if the absorbance A of the sample is less than 0.1, and moreover, if the rate of proton binding in the excited state can be neglected, the total fluorescence signal $F(\lambda_{ex},\lambda_{em}, [H^+])$ at proton concentration $[H^+]$, due to excitation at λ_{ex} and observed at emission wavelength λ_{em} can be expressed by[21,22]

$$F(\lambda_{ex},\lambda_{em},[H^+]) = \frac{F_{max}[H^+]^n + F_{min}K_a}{K_a + [H^+]^n} \qquad (16)$$

where F_{min} stands for the fluorescence signal of the basic form of the pH indicator (**2***), and F_{max} denotes the fluorescence signal of the acidic form of the pH indicator (**1***). F_{min} and F_{max} thus correspond to the fluorescence signals at *min*imum and *max*imum H^+ concentration, respectively. Fitting eq 16 to the fluorescence data $F(\lambda_{ex},\lambda_{em},[H^+])$ as a function of $[H^+]$ yields values for K_a, n, F_{min}, and F_{max}.

2.4. Determination of K_a from Ratiometric Fluorimetric Titration. Because large spectral shifts are observed in the fluorescence excitation spectra, the *ratiometric* method (eq 17, see ref 22) can be used to estimate values of K_a. In the excitation ratiometric method, one measures $R = F(\lambda_{em},\lambda_{ex}{}^1)/F(\lambda_{em},\lambda_{ex}{}^2)$ at a common emission wavelength, λ_{em}, and two different excitation wavelengths, $\lambda_{ex}{}^1$ and $\lambda_{ex}{}^2$. R_{min} and R_{max} correspond to the ratios at *min*imal and *max*imal $[H^+]$, respectively, and $\xi = F_{min}(\lambda_{em},\lambda_{ex}{}^2)/F_{max}(\lambda_{em},\lambda_{ex}{}^2)$.

$$R = \frac{R_{max}[H^+]^n + R_{min}K_a\xi}{K_a\xi + [H^+]^n} \qquad (17)$$

Fitting nonlinear eq 17 to the excitation ratiometric fluorescence data R as a function of $[H^+]$ yields values for $K_a\xi$, n, R_{min}, and R_{max}. Because $\xi(\lambda_{em},\lambda_{ex}{}^2)$—the ratio of the fluorescence signal of phenolate form (**2**) of BCECF over that of the phenol form (**1**) at the indicated excitation and emission wavelengths—is experimentally accessible, a value for K_a can be recovered from ratiometric excitation fluorescence data.

3. Experimental Section

3.1. Materials and Preparation of Solutions. The fluorescent pH indicator BCECF acid [2′,7′-bis-(2-carboxyethyl)-5-(and-6)-carboxyfluorescein, mixed isomers] was obtained from Invitrogen-Molecular Probes (Eugene, OR). For the preparation of phosphate buffer ($pK_a^B = 6.8$ at 20 °C) solutions, the following salts were used: $NaH_2PO_4{\cdot}H_2O$ (Fluka, puriss. p.a.) and $Na_2HPO_4{\cdot}7H_2O$ (Fluka, puriss. p.a.). To adjust the pH of the buffer solutions, 0.1 and 0.01 M solutions of HCl and NaOH were used. HCl (Aldrich, 1 N solution) and NaOH (Aldrich, platelets) were of spectroscopic grade quality. MOPS (SigmaUltra, > 99.5%) and TRIS (99.9% ultrapure grade) were purchased from Sigma-Aldrich. All the chemicals were used as received without further purification. All the measurements were performed using Milli-Q water as solvent. BCECF solutions for time-resolved fluorescence measurements were prepared by diluting a stock solution so that the absorbance of the final solutions at λ_{ex} was lower than 0.1. For the time-resolved fluorescence experiments, three BCECF solutions were prepared in the absence of buffer characterized by the pH values of 6.65, 7.58, and 12.21. In the presence of phosphate buffer ($C^B = 0.1$ M), seven solutions were prepared with the following pH values: 5.88, 6.21, 6.65, 6.84, 7.01, 7.48, and 7.78. Finally, five solutions were prepared characterized by the same pH (6.80) in the presence of phosphate buffer with $C^B = 0.09$, 0.18, 0.27, 0.36, and 0.45 M. The solutions were not degassed.

3.2. Instrumentation. Absorption spectra were recorded on a GBC Cintra 10e UV/Vis spectrophotometer with a temperature-controlled cell holder. The pH of the solutions was measured just before recording each spectrum. All measurements were made at room temperature, using 10 × 10 mm^2 cuvettes.

Fluorescence titrations in the absence and the presence of pH buffer were performed on a SPEX Fluorolog at room temperature. The pH of the solutions was measured just before the fluorescence measurements. Corrected steady-state fluorescence emission spectra were recorded by exciting samples at 505 and 490 nm, whereas excitation spectra were recorded by detecting the fluorescence at 535 nm.

Fluorescence decay traces of BCECF in the absence and in the presence of phosphate buffer were recorded by the single-photon timing method.[9,10] The second harmonic of a Ti:Sapphire laser (Tsunami, Spectra Physics) was used to excite the samples at 488 nm with a repetition rate of 4.09 MHz. Details of the instrumentation used[23] and experimental procedures[24] have been described elsewhere. Fluorescence decay histograms were collected in 4096 channels using 10 × 10 mm^2 cuvettes. The time increment per channel was 6.2 ps. Histograms of the instrument response functions (using LUDOX scatterer) and sample decays were recorded until they typically reached 10^4 counts in the peak channel. The total width at half-maximum of the instrument response function was ∼60 ps. The absorbance at the excitation wavelength was always below 0.1. Fluorescence decays were recorded at three λ_{em} (520, 540, and 560 nm) for the samples without buffer ($C^B = 0$ M) and samples at constant pH (6.80). For the samples characterized by a constant phosphate concentration, C^B (0.1 M), decays were collected at four λ_{em} (520, 540, 560, and 580 nm). The total number of collected fluorescence decays was 52. From those decays, 9 corresponded to samples without buffer, 15 to samples at the same pH (6.80) and different C^B, and 28 to samples at the same C^B (0.1 M) and different pH. All lifetime measurements were performed on nondegassed samples at 20 °C.

3.3. Data Analysis of Time-Resolved Fluorescence. The global compartmental analysis of the fluorescence decay surface of species undergoing excited-state processes in the presence of added buffer was implemented in a general global analysis program using Gaussian-weighted nonlinear least-squares fitting based on Marquardt−Levenberg minimization.[25] Any of the fitting parameters can be kept fixed during the fitting, or may be freely adjustable to seek optimum values.

Consider the excited-state process in the presence of added buffer as depicted in Scheme 1. The global (linkable) fitting parameters are k_{01}, k_{02}, k_{21}, k_{12}^B, k_{21}^B, $\tilde{b}_1$, and $\tilde{c}_1$. The rate constants k_{ij} can be linked over the whole fluorescence decay surface, the $\tilde{b}_1$ parameters can be linked for the samples at the same pH and λ_{ex}, and the $\tilde{c}_1$ parameters can be linked for the samples at the same λ_{em}. The only local (nonlinkable) fitting parameters are the scaling factors κ (eq 1).

At each pH and C^B, the values of [R] and [RH] of the buffer with acidity constant K_a^B were computed according to eq 13.

Assigning initial guesses to the rate constants k_{01}, k_{02}, k_{21}, k_{12}^{B}, and k_{21}^{B} allows one to construct the compartmental matrix **A** (eq 2) for each decay trace. The starting value for all rate constants k_{ij} was 1×10^9 (M^{-1}) s^{-1}; for $\tilde{b}_1$ and $\tilde{c}_1$, the initial guesses were 0 and/or 1. The generalized global mapping table approach described previously[26] allows one to analyze simultaneously experiments done at different λ_{ex} and λ_{em}, at multiple timing calibrations, and at different pH and C^B values.

The fitting parameters were determined by minimizing the global *reduced* chi-square χ_g^2:

$$\chi_g^2 = \sum_{l}^{q} \sum_{i} w_{li}(y_{li}^{o} - y_{li}^{c})^2/\nu \qquad (18)$$

where the index l sums over q experiments, and the index i sums over the appropriate channel limits for each individual experiment. y_{li}^{o} and y_{li}^{c} denote respectively the experimental and fitted values corresponding to the ith channel of the lth experiment, and w_{li} is the corresponding statistical weight. ν represents the number of degrees of freedom for the entire multidimensional fluorescence decay surface. It is essential that all fitting parameters are subject to simple range constraints on their values. The problem of minimizing χ_g^2 can be stated mathematically as follows: minimize $\chi_g^2(x)$ for all x, $x \in R^n$ subject to $s_j \leq x_j \leq t_j$, with $j = 1, 2, ..., n$ and n being the number of adjustable parameters. This format assumes that lower and upper constraints exist on all fitting parameters. Restrictions on the values of a particular fitting parameter j can be removed by allowing very large negative and positive values of s_j and t_j, respectively. For all rate constants and local scaling factors s_j was set at 0; the default constraints on $\tilde{b}_1$ and $\tilde{c}_1$ were $-0.2 \leq \tilde{b}_1, \tilde{c}_1 \leq 1.2$. Small, negative s_j prevent oscillations in the nonlinear least-squares search, which would occur if the values of the fitting parameters were forced to be nonnegative. These constraints can be adjusted, if necessary.

The goodness-of-fit was judged for each fluorescence decay trace separately as well as for the global fluorescence decay surface. The statistical criteria to assess the quality of the fit comprised both graphical and numerical tests, and have been described elsewhere.[27]

4. Results and Discussion

4.1. Absorption Spectroscopy. The visible absorption spectra of aqueous solutions of BCECF in the pH range between 4.6 and 9.2 have been recorded at various phosphate buffer concentrations and ionic strengths (by adding KCl at different concentrations to the buffer solutions). Figure 2a shows an example of the visible absorption spectra recorded for BCECF buffered solutions ($C^B = 0.1$ M phosphate) in the presence of 0.1 M added KCl, at different pH values. In basic solution, the spectrum is essentially composed of a band characterized by a maximum at 502 nm and a small shoulder around 475 nm. When the pH decreases, the peak at 502 nm is blue-shifted, its absorbance value decreases, whereas the shoulder becomes more pronounced. At pH around 5.0, the spectrum shape changes and is composed of two maxima: one at 490 nm and the other at 452 nm. In the pH range 5.5−9.0, only one isosbestic point (namely, at 470 nm) can be clearly distinguished. At pH values below 5.0, the isosbestic point disappears indicating that other different species are involved in the ionic equilibrium. The experimental absorption spectra of BCECF solutions at pH values ranging between 5.5 and 9.0 show that only one pH-induced transition at near-neutral pH (characterized by one ground-state pK_a) is involved. Because the ground-state acidity of the four carboxylic groups of BCECF is higher than the acidity of the xanthene-phenolic OH group, the four carboxylic groups are deprotonated at pH values higher than 5.0, and the observed transition at near-neutral pH is due to ground-state proton exchange at the phenol group. As in fluorescein, the absorption of the phenolate anion of BCECF is red-shifted and has an increased molar absorption coefficient relative to the phenolic acid form.

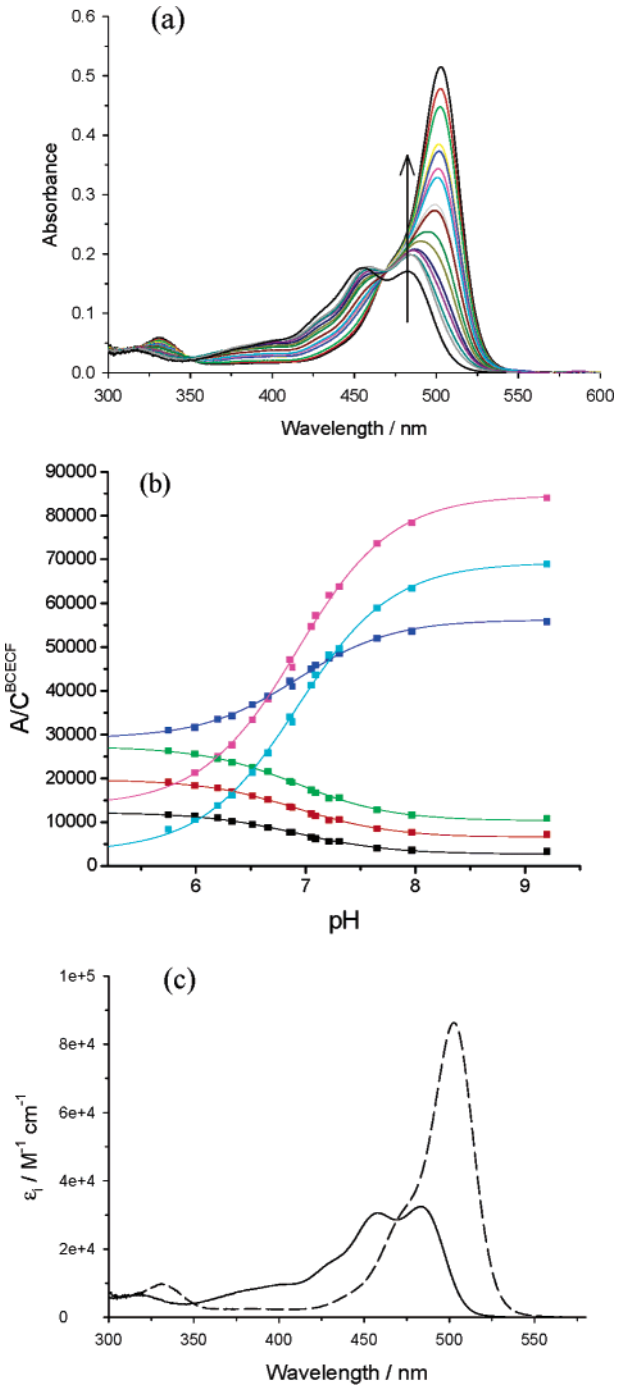

Figure 2. (a) Absorption spectra of BCECF (at 6×10^{-6} M) in phosphate buffer ($C^B = 0.1$ M) in the presence of 0.1 M KCl, at pH values between 4.63 (breaking the isosbestic point) and 9.20. The arrow indicates increasing pH values. (b) Global fitting of the A/C^{BCECF} vs pH curves of BCECF solutions in phosphate buffer ($C^B = 0.1$ M) in the presence of 0.1 M KCl. The wavelengths shown are 420 (black), 440 (red), 450 (green), 490 (blue), 500 (magenta), and 510 nm (cyan). (c) Recovered molar absorption coefficients of the BCECF tetraanion (solid line, structure **1** in Figure 1) and pentaanion (dashed line, structure **2** in Figure 1) in 0.05 M phosphate buffer and 0.05 M KCl.

TABLE 1: Apparent pK_a Values of BCECF Determined by Absorbance (pK_a[a]) (eq 15), and Direct (eq 16) and Ratiometric (eq 17) Fluorimetric Titrations (pK_a[b]) in the Absence/Presence of Added Buffer and Added KCl[c]

concentration of added buffer and KCl	μ	pK_a[a]	pK_a[b]
0 M buffer + 0 M KCl	0		7.78 ± 0.03
0.01 M phosphate + 0 M KCl	0.02		7.39 ± 0.01
0 M buffer + 0.1 M KCl	0.1		7.18 ± 0.06
0.1 M TRIS + 0 M KCl	0.1	7.266 ± 0.008	
0.01 M phosphate + 0.1 M KCl	0.12		7.10 ± 0.01
0.01 M MOPS + 0.1 M KCl	0.11		7.02 ± 0.02
0.05 M phosphate + 0 M KCl	0.1		7.13 ± 0.01
0.05 M phosphate + 0.05 M KCl	0.15	7.043 ± 0.005	
0.05 M phosphate + 0.1 M KCl	0.2		7.00 ± 0.01
0.05 M MOPS + 0.1 M KCl	0.15		6.83 ± 0.02
0.1 M phosphate + 0 M KCl	0.2		7.00 ± 0.01
0.1 M phosphate + 0.1 M KCl	0.3	6.922 ± 0.008	6.90 ± 0.01
0.1 M MOPS + 0.1 M KCl	0.2		6.97 ± 0.02
0.1 M phosphate + 0.5 M KCl	0.7	6.756 ± 0.005	
0.1 M phosphate + 1 M KCl	1.2	6.706 ± 0.009	

[a] Determined from absorbance measurements. [b] Determined from fluorimetric titrations. [c] The values of the ground-state acidity constants K_a measured from emission and excitation spectra are in excellent agreement. The ionic strength values μ were calculated for solutions at 20 °C and pH 6.8 for phosphate buffer, pH 7.2 for MOPS, and pH 8.1 for TRIS (these pH values correspond to the pK_a^B values of the respective buffers at 20 °C).

To determine the ground-state pK_a and the molar absorption coefficients, the approach described in section 2.2 was performed. A typical A vs pH vs λ_{abs} data surface at each buffer concentration and ionic strength was composed of 15 pH values, three different BCEFC concentrations, and 545 λ_{abs} values between 300 and 570 nm. Note that the spectra corresponding to the lowest pH values were removed from the analysis, because they did not have the isosbestic point (see Figure 2a), suggesting a third species is involved in the equilibrium. Beer's law for two prototropic species turned out to be the best model to fit the experimental absorption data. A three-species model resulted in a higher parameter dependency and did not improve the statistical goodness-of-fit parameters. Plots of the individual A/C^{BCECF} vs pH curves at different wavelengths and the generated curves from the fitting are shown in Figure 2b. In the data surface fitting process the estimated parameter values were independent of the initial guesses assigned to these parameters. The recovered pK_a^{app} values along with the associated errors are indicated in Table 1. The recovered molar absorption coefficients ϵ_1 of the tetraanionic (structure **1** in Figure 1) and ϵ_2 of the pentaanionic (structure **2** in Figure 1) forms were practically independent of the ionic strength. Figure 2c shows, as an example, the recovered values of the molar absorption coefficients of **1** and **2** in 0.05 M phosphate buffer and 0.05 M KCl.

4.2. Fluorimetric Titration. The value of the acidity constant of BCECF, measured by direct fluorimetric titrations and reported in the literature (apparent pK_a of 6.96 from excitation spectra and 6.98 from emission spectra, measured at $\lambda_{ex} = 500$ nm and $\lambda_{em} = 530$ nm),[4] has been obtained from experiments in the presence of 10 mM MOPS buffer and added salts (130 mM KCl, 10 mM NaCl, 1 mM $MgSO_4$). We performed a direct fluorimetric titration in the absence of any buffer or salt and found a much higher value, namely pK_a = 7.78 ± 0.03. A representative example of the emission spectra of BCECF as a function of pH in 100 mM KCl and in the absence of added buffer is shown in Figure 3a. The fluorescence emission decreases at lower pH values, in agreement with previous observations.[4] To investigate the influence of added salt and buffer on K_a, we then performed fluorimetric titrations as a function of different concentrations of added buffer (phosphate and MOPS) in the absence and presence of 100 mM KCl. The average pK_a values obtained by fitting eq 16 (direct fluorimetric titration) or eq 17 (ratiometric excitation fluorimetric titration) to the pH dependent fluorescence data are compiled in Table 1. Figure 3b displays the best fit of eq 16 with $n = 1$ to the fluorescence emission titration data of Figure 3a. Analogous results were obtained from fluorescence excitation titrations (Figure 3c). Figure 3d displays the best fit of eq 17 with $n = 1$ to the *ratiometric* excitation fluorimetric titration data obtained from the spectra of Figure 3c ($\lambda_{em} = 535$ nm, $\lambda_{ex}^1/\lambda_{ex}^2 = 500/435$ nm).

It is evident that, upon addition of even a small amount of buffer (C^B = 10 mM phosphate buffer), the apparent K_a increases significantly (pK_a decreases from ~7.8 to ~7.4). Increasing C^B further to 50 mM and 100 mM phosphate buffer leads to an additional decrease of pK_a to ~7.1 and 7.0, respectively. Addition of salt causes an extra decrease of pK_a. The effect of decrease of pK_a is more pronounced at low C^B and appears to level off at high C^B. Similar effects were found for MOPS buffer and KCl. The value of ~7.0 for pK_a measured under physiological salt conditions[4] agrees well with those found in our investigation. Theoretically, the change of the ground-state acidity constant K_a value with increasing C^B is related to an increase of ionic strength μ of the solution. We deal with this in the following section.

4.3. Influence of Ionic Strength. The BCECF prototropic species of interest are the tetraanion (structure **1** in Figure 1) and the pentaanion (structure **2** in Figure 1), which are extremely ionic strength sensitive. Because the ionic strength affects the ratio of penta and tetraanion concentrations and, hence, the BCECF optical signal, a comprehensive study of the dependence of K_a on the ionic strength μ is of a major interest for using this fluorophore as a pH probe.

The Hendersson−Hasselbalch equation, which relates pH with concentration of the prototropic species, applied to the studied equilibrium of BCECF at near-neutral pH is the following:[28]

$$\mathrm{pH} = \mathrm{p}K_a + \log\left(\frac{[\mathbf{2}]}{[\mathbf{1}]}\right) + \log\left(\frac{f_2}{f_1}\right) - \log\left(a_{H_2O}\right) \quad (19)$$

where [**1**] and [**2**] stand for the concentrations of the tetraanion (**1**) and the pentaanion (**2**), respectively, of BCECF (see Figure 1). f_1 and f_2 denote the activity coefficients of the respective species, and a_{H_2O} is the water activity. The apparent pK_a^{app} is given by

$$\mathrm{p}K_a^{app} = \mathrm{p}K_a + \log\left(\frac{f_2}{f_1}\right) - \log\left(a_{H_2O}\right) \quad (20)$$

and depends on the ratio of the activity coefficients f_i.

The estimated pK_a values plotted, for both the absorbance and fluorescence approaches, as a function of the ionic strength μ, are shown in Figure 5. The change of the apparent ground-state acidity constant pK_a^{app} value with increasing ionic concentration μ can be related with the increase of ionic strength of the solution. Therefore, we used a semiempirical function based on the extended Debye−Hückel equation to relate f_1 and f_2 with μ. Using this approach, the activity coefficients may be represented as:

$$\log f_i = \frac{-Az_i^2\sqrt{\mu}}{1 + \dot{a}_i B\sqrt{\mu}} + L_i\mu \quad (21)$$

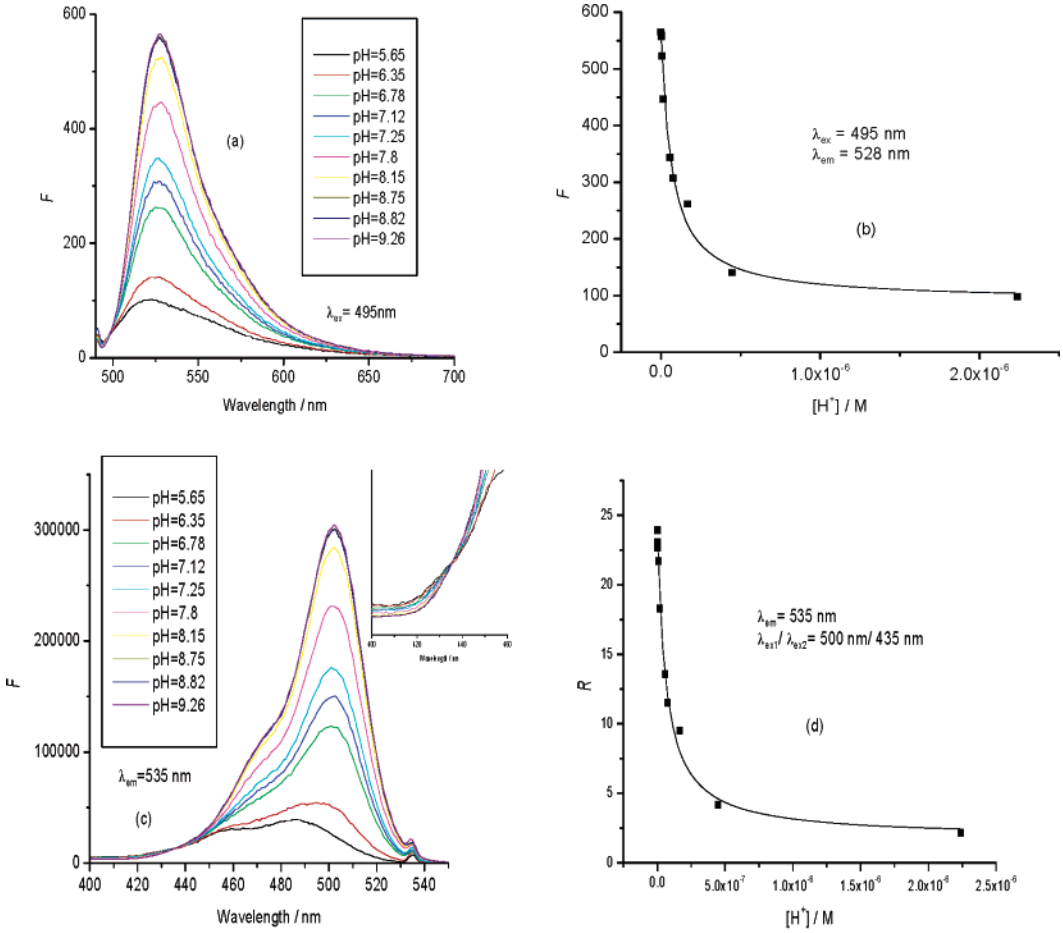

Figure 3. (a) Fluorescence emission spectra (λ_{ex} = 495 nm) of BCECF as a function of pH in 100 mM KCl without buffer. (b) The solid line represents the best fit of eq 16 with $n = 1$ to the *direct* emission fluorimetric titration data of BCECF obtained from the spectra of Figure 3a (λ_{ex} = 495 nm, λ_{em} = 528 nm). (c) Corresponding fluorescence excitation spectra (λ_{em} = 535 nm). (Inset) Enlargement of the pseudo-isoemissive point of BCECF at 435 nm. (d) Best fit of eq 17 with $n = 1$ to the *ratiometric* excitation fluorimetric titration data obtained from the spectra of Figure 3c (λ_{em} = 535 nm, $\lambda_{ex}^1/\lambda_{ex}^2$ = 500/435 nm).

In this equation, also called the Truesdell−Jones equation,[29] L_i is an adjustable parameter, typical values for A and B at room temperature and atmospheric pressure are 0.51 and 0.33, respectively, $\dot{a}_i$ stands for the ionic radius in Angstroms, and z_i is the ionic charge. Substituting eq 21 into 19, and assuming a similar radius for **1** and **2** (i.e., $\dot{a}_1 = \dot{a}_2 = \dot{a}$), leads to

$$pK_a^{app} = pK_a - \left(A(z_2^2 - z_1^2)\frac{\sqrt{\mu}}{1 + \dot{a}B\sqrt{\mu}} + L^*\mu\right) - \log(a_{H_2O}) \quad (22)$$

in which L^* represents a composite, adjustable parameter of the individual L_i. The experimental pK_a values, estimated by both absorption and fluorescence methods, were fitted to eq 22 using nonlinear least-squares fitting. A value of 9 Å was used for the ionic radius $\dot{a}$. Because the experimental molecular radius of BCECF is not available, we have built a model of the molecule using the Sybyl program[30] to calculate the size and the molecular radius of the BCECF compound. To this purpose, appropriate fragments from the Sybyl libraries were used to build the molecule, and partial atomic charges were calculated by means of the Gasteiger−Marsili method.[31] The Tripos force field[32] was used in the energy calculation and the geometry was optimized using the Powel[33] method, until the energy gradient was smaller than 0.05 kcal mol^{-1} Å^2. Figure 4 represents the solvent-accessible surface calculated on the optimized geometry of the 5-substituted isomer (see Figure 1) of BCECF by means of the above-mentioned program, as well as some significant distances in the molecule. Calculated values for the surface and the volume of this molecule were 435.3 Å^2 and 452.5 Å^3, respectively. Measured distances between the center of mass (C-7) and several distal points of the molecule range from 6.6 to 8.6 Å, smaller than or similar to the proposed 9 Å radius. Comparable values were found for the 6-substituted isomer (see Figure 1) of BCECF. Because it can be expected that the hydrated radius should be significantly larger than the radius

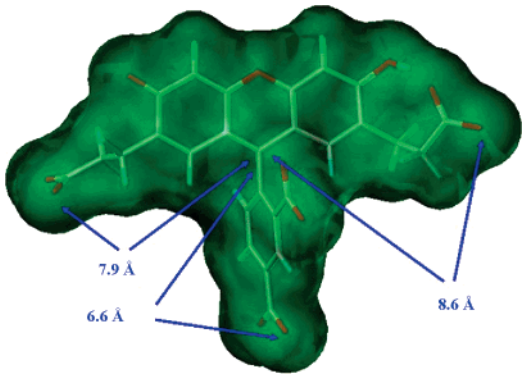

Figure 4. Solvent accessible surface calculated on the optimized geometry of BCECF by means of the Sybyl programs. The value of the surface and the volume calculated are of 435.3 Å^2 and 452.5 Å^3, respectively. Arrows indicate distances measured between the center of mass of the molecule (that almost coincides with C7) and several distal points of the molecule.

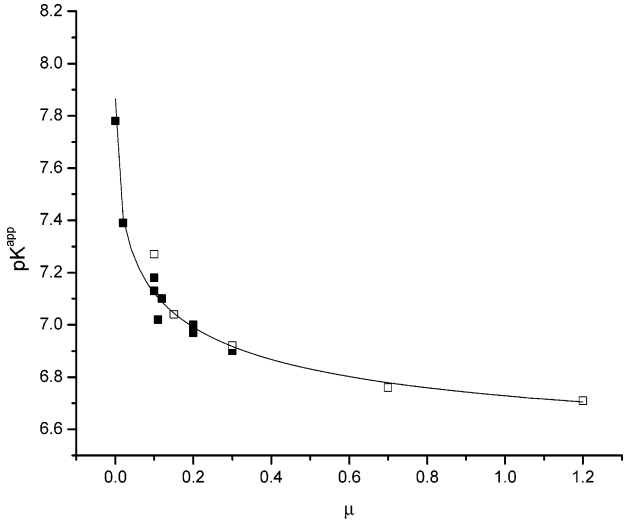

Figure 5. Graphical representation of the dependence of the estimated pK_a^{app} values of BCECF on ionic strength (μ). The open symbols represent the absorption measurements and the black squares correspond to the fluorescence measurements. Solid line: Global fitting of eq 22.

of the same isolated ion, the average value of 9 Å used in the fitting seems to be reasonable. Figure 5 shows the fitting curve, from which an estimated pK_a value of 7.87 ± 0.02 ($r^2 = 0.96$) was obtained.

4.4. Time-Resolved Fluorescence. First, each fluorescence decay trace, measured under different experimental conditions (i.e., absence or presence of phosphate buffer with total concentration C^B, different pH values and λ_{em},), was analyzed individually as a biexponential function in terms of decay times τ_i and associated preexponential factors α_i ($i = 1, 2$). Such single-curve analysis not only discloses the number of needed exponential terms but also tests the quality of the experimental decay data and allows one to weed out substandard experimental decay data. Traces that gave unacceptable fits as biexponentials were eliminated from further analysis.

Second, classical global biexponential analyses in terms of τ_i and α_i were performed incorporating in a single decay surface curves collected at the same pH and C^B, but at different λ_{em}. The decay times τ_i were linked (held in common) for decay traces measured at different λ_{em}. It can be expected that such a global analysis would estimate the $\{\tau_i, \alpha_i\}$ values with higher accuracy and precision than single-curve analysis. Unfortunately, the decay times τ_1 and τ_2 of BCECF are rather closely spaced with a small contribution α_1 of the shorter decay time corresponding to the tetraanionic form **1***. Thus, the two global biexponential analyses of fluorescence decay surfaces containing three traces measured as a function of λ_{em} (520, 540, and 560 nm) at $C^B = 0$ M and pH 6.65 and 7.58, and the five global analyses of fluorescence decay surfaces with three decay traces collected at pH 6.80 and different C^B (0.09, 0.18, 0.27, 0.36, and 0.45 M) as a function of λ_{em} (520, 540, and 560 nm) could not recover reliable $\{\tau_i, \alpha_i\}$ estimates. That could be ascertained from the wide range of $\{\tau_i, \alpha_i\}$ values estimated by global fitting as a function of the initial parameter guesses. Especially imprecise were the values $\{\tau_1, \alpha_1\}$ associated with the tetraanionic form **1***. The imprecise estimates corresponding to **1*** were also observed for the seven global biexponential analyses of fluorescence decay surfaces containing four traces as a function of λ^{em} (520, 540, 560, and 580 nm) at $C^B = 0.1$ M and pH 5.88, 6.21, 6.65, 6.84, 7.01, 7.48, and 7.78. However, global analysis of the fluorescence decay surface ($\chi_g^2 = 1.08$) including nine curves corresponding to $C^B = 0$ M at pH 6.65, 7.58, and 12.21 at $\lambda_{em} = 520$, 540, and 560 nm provided us with reliable decay time estimates: $\tau_1 = 2.95 \pm 0.02$ ns and $\tau_2 = 3.89 \pm 0.01$ ns, corresponding to ($k_{01} + k_{21} = 3.39 \times 10^8$ s^{-1}) and $k_{02} = 2.57 \times 10^8$ s^{-1}, respectively. Global curve-fitting of those nine decay curves resulted in the same parameter estimates with the same high precision, regardless of the initial $\{\tau_i, \alpha_i\}$ guesses. The decays at pH 12.21 were monoexponential with a lifetime τ_2 corresponding to the pentaanionic form **2***, as predicted by eq 14. These lifetime values of the tetraanionic (**1***) and pentaanionic (**2***) forms of BCECF are quite close to the values of 2′,7′-difluorofluorescein monoanion (3.40 ± 0.01 ns) and dianion (4.05 ± 0.02 ns) reported elsewhere.[19] This supports the idea of the same chromophoric group in the xanthene moiety of BCECF compared to fluorescein.

TABLE 2: Rate Constant Values Estimated by Global Compartmental Analysis of the Fluorescence Decay Surface Containing 44 Decay Traces of BCECF in Aqueous Solution at pH between 5.88 and 12.21, in the Absence ($C^B = 0$ M) and Presence of Phosphate Buffer (C^B between 0.09 and 0.45 M)

k_{01} (s^{-1})	$(3.40 \pm 0.03) \times 10^8$
k_{02} (s^{-1})	$(2.56 \pm 0.03) \times 10^8$
k_{21} (M^{-1} s^{-1})	$(1 \pm 1) \times 10^6$
k_{12}^B (M^{-1} s^{-1})	$(1.4 \pm 0.4) \times 10^8$
k_{21}^B (M^{-1} s^{-1})	$(4.3 \pm 0.5) \times 10^7$

Finally, we collected in a single decay surface all measured (52) decays and analyzed them globally in terms of the rate constants k_{ij} and the spectral parameters $\tilde{b}_1$ and $\tilde{c}_1$. The linked fitting parameters were k_{01}, k_{02}, k_{21}, k_{12}^B, k_{21}^B, $\tilde{b}_1$, and $\tilde{c}_1$, whereas the only local (nonlinkable) fitting parameters were the scaling factors κ.[24] Due to the imperfection of certain traces, the global reduced χ_g^2 remained somewhat elevated (1.14). To obtain more reliable estimates that would better fit the experimental data, we removed from the decay surface eight traces that had local $\chi^2 > 1.2$, corresponding to decays that gave poor-quality biexponential fits in the previous global analyses. The resulting decay surface with 44 traces was analyzed globally in terms of the rate constants k_{ij} and the spectral parameters $\tilde{b}_1$ and $\tilde{c}_1$. This global fit was slightly better than that with 52 traces (as judged from $\chi_g^2 = 1.09$ and the plots of the weighted residuals and the autocorrelation functions) and yielded very similar k_{ij} (except for k_{21} and k_{12}^B), $\tilde{b}_1$, and $\tilde{c}_1$ estimates. The estimated rate constants are compiled in Table 2. The estimated k_{21} and k_{12}^B values in the global fit with 52 curves are: $k_{21} = (2 \pm 2) \times 10^6$ M^{-1} s^{-1} and $k_{12}^B = (5 \pm 2) \times 10^7$ M^{-1} s^{-1}. Particularly for k_{21} no reliable value could be obtained.

We discussed above the critical influence of the ionic strength μ on the ground-state pK_a and the apparent pK_a calculated through steady-state fluorescence measurements. Indeed, the ionic strength may affect the determination of the rate constants as well. Therefore, the recovered rate constant values should be considered as average values over the narrow ionic strength range studied in the time-resolved fluorescence measurements. Previously, we developed the correct model to take into account ionic strength variations in the global compartmental analysis,[19] but we concluded this entailed such a complex methodology that it may not be worth considering. We also note the high associated error in the determination of k_{21}.

To test the validity of the estimated rate constants, the decay times τ_1 and τ_2 (eq 12) were calculated (according to eqs 9−13) using the globally estimated rate constant values $\{k_{01}, k_{02}, k_{21}, k_{12}^B, k_{21}^B\}$, C^B, pH, and pK_a^B of phosphate buffer at 20 °C (6.8). A satisfactory agreement between the decay times $\{\tau_1, \tau_2\}$ calculated as a function of pH at $C^B = 0.1$ M and those obtained by global biexponential fitting was found (Figure 6). For the

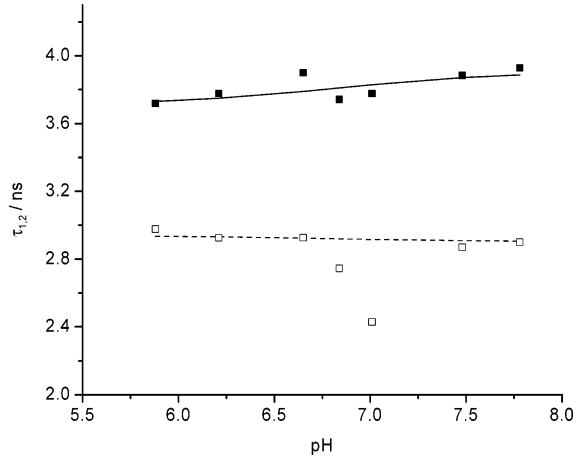

Figure 6. Dependence of the decay times τ_1 and τ_2 on pH at constant total buffer concentration ($C^B = 0.1$ M). The estimated τ_1 (□) and τ_2 (■) have been obtained by global biexponential curve-fitting of fluorescence decay surfaces containing four decays collected at $\lambda_{em} =$ 520, 540, 560, and 580 nm. The decay times τ_1 (dashed line) and τ_2 (solid line) have been calculated according to eqs 9−13, using the globally estimated rate constant values $\{k_{01}, k_{02}, k_{21}, k_{12}^B, k_{21}^B\}$ compiled in Table 2, C^B, pH, and pK_a^B(6.8) of phosphate buffer at 20 °C.

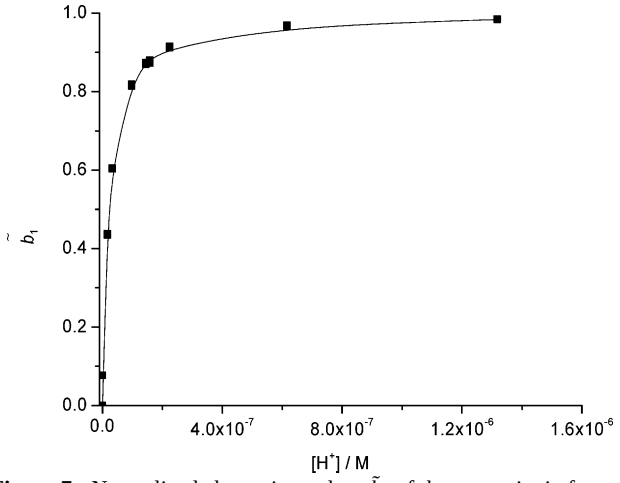

Figure 7. Normalized absorption values $\tilde{b}_1$ of the tetraanionic form **1** of BCECF as a function of pH. The black squares represent values estimated by global compartmental analysis. The solid line corresponds to the best fit of eq 5 to the estimated values.

samples without added buffer, a perfect accordance between the two sets of decay times $\{\tau_1, \tau_2\}$ was obtained (calculated values: $\tau_1 = 2.94$ ns and $\tau_2 = 3.91$ ns). The poor correlation between the calculated and estimated τ_1 values as a function of pH at $C^B = 0.1$ M (Figure 6) and of C^B at pH 6.80 could be anticipated, because it is more difficult to estimate accurately the shorter decay time τ_1 due to its lower contribution. Indeed, its contribution almost vanishes at higher pH (see eq 14) and higher buffer concentrations ($C^B \geq 0.27$ M).

The values of $\tilde{b}_1$ (normalized absorbance of the tetraanion **1**) estimated by global compartmental analysis are depicted in Figure 7 as a function of proton concentration. Nonlinear curve-fitting of eq 5 to the experimental data yielded an estimated value of $(2.2 \pm 0.1) \times 10^{-8}$ for $K_a\epsilon_2(\lambda_{ex})/\epsilon_1(\lambda_{ex})$ at $\lambda_{ex} = 488$ nm with excellent correlation ($r^2 = 0.99$). Using the $\epsilon_2(\lambda_{ex})/\epsilon_1(\lambda_{ex})$ ratio recovered from the absorption measurements (1.61), a value of p$K_a = 7.86$ is recovered, which is in excellent agreement with the result obtained by other methods.

5. Conclusions

The apparent pK_a of the phenolic group in BCECF has been obtained by means of absorbance and fluorescence measurements at different ionic strength values. Its dependence with ionic strength has been explored. Even a small amount of added buffer increases drastically the apparent acidity constant. We have developed a simple approach taking into account the variations in the activity factors, having resolved a semiempirical equation describing the apparent pK_a behavior with ionic strength. Time-resolved fluorescence measurements in the absence and presence of phosphate buffer and global compartmental analysis of the fluorescence decay surface have enabled us to estimate the following excited-state rate constants: $k_{01} = 3.4 \times 10^8$ s^{-1}, $k_{02} = 2.6 \times 10^8$ s^{-1}, $k_{21} \approx 1 \times 10^6$ M^{-1} s^{-1}, $k_{12}^B = 1.4 \times 10^8$ M^{-1} s^{-1}, and $k_{21}^B = 4.3 \times 10^7$ M^{-1} s^{-1}.

Acknowledgment. We thank Ms. A. Stefan for technical help with the time-resolved fluorescence experiments. We are grateful to the University Research Fund of the K.U.Leuven for IDO-grant IDO/00/001 and postdoctoral fellowships to W. Qin and N. Basarić. This work was supported by grant G.0320.00 of the Fonds voor Wetenschappelijk Onderzoek − Vlaanderen and in part by grant BQU2002-01311 from the Spanish Ministry of Science and Technology.

References and Notes

(1) Haugland, R. P. *The Handbook. A Guide to Fluorescent Probes and Labeling Technologies*, 10th ed.; Invitrogen−Molecular Probes: Eugene, OR, 2005; pp 935−955.
(2) Zanker, V.; Peter, W. *Chem. Ber.* **1958**, *91*, 572−580.
(3) Diehl, H.; Horchak-Morris, N. *Talanta* **1987**, *34*, 739−741.
(4) Rink, T. J.; Tsien, R. Y.; Pozzan, T. *J. Cell Biol.* **1982**, *95*, 189−196.
(5) Paradiso, A. M.; Tsien, R. Y.; Machen, T. E. *Proc. Natl. Acad. Sci. U.S.A.* **1984**, *81*, 7436−7440.
(6) Kowalczyk, A.; Boens, N.; Meuwis, K.; Ameloot, M. *Anal. Biochem.* **1997**, *245*, 28−37.
(7) Kowalczyk, A.; Boens, N.; Ameloot, M. *Methods Enzymol.* **1997**, *278*, 94−113.
(8) Szmacinski, H.; Lakowicz, J. R. *Anal. Chem.* **1993**, *65*, 1668−1674.
(9) O'Connor, D. V.; Phillips, D. *Time-Correlated Single Photon Counting*; Academic Press: London, 1984.
(10) Boens, N. In *Luminescence Techniques in Chemical and Biochemical Analysis*; Baeyens, W. R. G., De Keukeleire, D., Korkidis, K., Eds.; Marcel Dekker: New York, 1991; pp 21−45.
(11) Knutson, J. R.; Beechem, J. M.; Brand, L. *Chem. Phys. Lett.* **1983**, *102*, 501−507.
(12) Beechem, J. M.; Ameloot, M.; Brand, L. *Anal. Instrum.* **1985**, *14*, 379−402.
(13) Janssens, L. D.; Boens, N.; Ameloot, M.; De Schryver, F. C. *J. Phys. Chem.* **1990**, *94*, 3564−3576.
(14) Beechem, J. M.; Ameloot, M.; L. Brand, L. *Chem. Phys. Lett.* **1985**, *120*, 466−472.
(15) Ameloot, M.; Beechem, J. M.; Brand, L. *Chem. Phys. Lett.* **1986**, *129*, 211−219.
(16) Ameloot, M.; Boens, N.; Andriessen, R.; Van den Bergh, V.; De Schryver, F. C. *J. Phys. Chem.* **1991**, *95*, 2041−2047.
(17) Beechem, J. M.; Gratton E.; Ameloot M.; Knutson J. R.; Brand L. In *Topics in Fluorescence Spectroscopy*, *Volume 2*: *Principles*; Lakowicz, J. R., Ed.; Plenum Press: New York, 1991; pp 241−305.
(18) Boens, N.; Basarić, N.; Novikov, E.; Crovetto, L.; Orte, A.; Talavera, E. M.; Alvarez-Pez, J. M. *J. Phys. Chem. A* **2004**, *108*, 8180−8189.
(19) Orte, A.; Crovetto, L.; Talavera, E. M.; Boens, N.; Alvarez-Pez, J. M. *J. Phys. Chem. A* **2005**, *109*, 734−747.
(20) Qin, W.; Basarić, N.; Boens, N. *J. Phys. Chem. A* **2005**, *109*, 4221−4230.
(21) Cielen, E.; Tahri, A.; Ver Heyen, K.; Hoornaert, G. J.; De Schryver, F. C.; Boens, N. *J. Chem. Soc., Perkin Trans. 2* **1998**, 1573−1580.
(22) Cielen, E.; Stobiecka, A.; Tahri, A.; Hoornaert, G. J.; De Schryver, F. C.; Gallay, J.; Vincent, M.; Boens, N. *J. Chem. Soc., Perkin Trans. 2* **2002**, 1197−1206.
(23) Maus, M.; Rousseau, E.; Cotlet, M.; Schweitzer, G.; Hofkens, J.; Van der Auweraer, M.; De Schryver, F. C.; Krueger, A. *Rev. Sci. Instrum.* **2001**, *72*, 36−40.
(24) Crovetto, L.; Orte, A.; Talavera, E. M.; Alvarez-Pez, J. M.; Cotlet, M.; Thielemans, J.; De Schryver, F. C.; Boens, N. *J. Phys. Chem. B* **2004**, *108*, 6082−6092.
(25) Program developed jointly by the Technology Institute of the Belarusian State University (Minsk, Belarus) and the Division of Molecular and Nanomaterials of the K. U. Leuven (Leuven, Belgium).

(26) Boens, N.; Janssens, L. D.; De Schryver, F. C. *Biophys. Chem.* **1989**, *33*, 77−90.
(27) Van den Zegel, M.; Boens, N.; Daems, D.; De Schryver, F. C. *Chem. Phys.* **1986**, *101*, 311−335.
(28) Weidgans, B. M.; Krause, C.; Klimant, I.; Wolfbeis, O. S. *Analyst* **2004**, *129*, 645−650.
(29) Langmuir, D. L. *Aqueous Environmental Geochemistry*; Prentice Hall: Upper Saddle River, NJ, 1997.
(30) SYBYL Molecular Modelling Software is available from Tripos Inc., 1699 S. Hanley Road, St. Louis, MO 63144-2913, http://www.tripos.com.
(31) (a) Gasteiger, J.; Marsili, M. *Tetrahedron* **1980**, *36*, 3219−3222. (b) Gasteiger, J.; Marsili, M. *Org. Magn. Reson.* **1981**, *15*, 353−360.
(32) Clark, M.; Cramer, R. D., III; Van Opdenbosch, N. *J. Comput. Chem.* **1989**, *10*, 982−1012.
(33) Powell, M. J. D. *Math. Prog.* **1977**, *12*, 241−254.